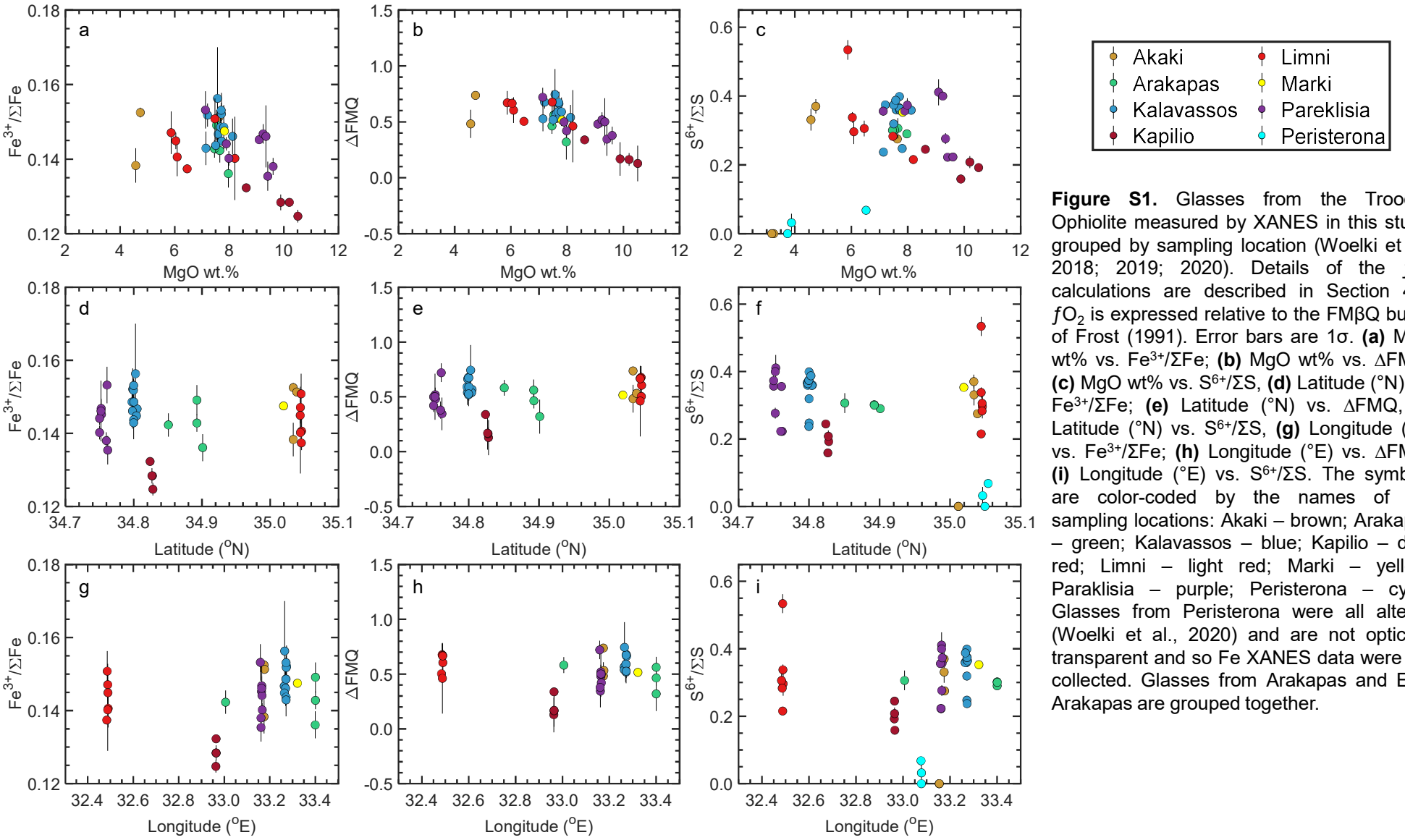

Figure S1. Glasses from the Troodos Ophiolite measured by XANES in this study, grouped by sampling location (Woelki et al., 2018; 2019; 2020). Details of the fO_2 calculations are described in Section 4.1. fO_2 is expressed relative to the FMβQ buffer of Frost (1991). Error bars are 1σ. **(a)** MgO wt% vs. $Fe^{3+}/\Sigma Fe$; **(b)** MgO wt% vs. ΔFMQ, **(c)** MgO wt% vs. $S^{6+}/\Sigma S$, **(d)** Latitude (°N) vs. $Fe^{3+}/\Sigma Fe$; **(e)** Latitude (°N) vs. ΔFMQ, **(f)** Latitude (°N) vs. $S^{6+}/\Sigma S$, **(g)** Longitude (°E) vs. $Fe^{3+}/\Sigma Fe$; **(h)** Longitude (°E) vs. ΔFMQ, **(i)** Longitude (°E) vs. $S^{6+}/\Sigma S$. The symbols are color-coded by the names of the sampling locations: Akaki – brown; Arakapas – green; Kalavassos – blue; Kapilio – dark red; Limni – light red; Marki – yellow; Paraklisia – purple; Peristerona – cyan. Glasses from Peristerona were all altered (Woelki et al., 2020) and are not optically transparent and so Fe XANES data were not collected. Glasses from Arakapas and East Arakapas are grouped together.

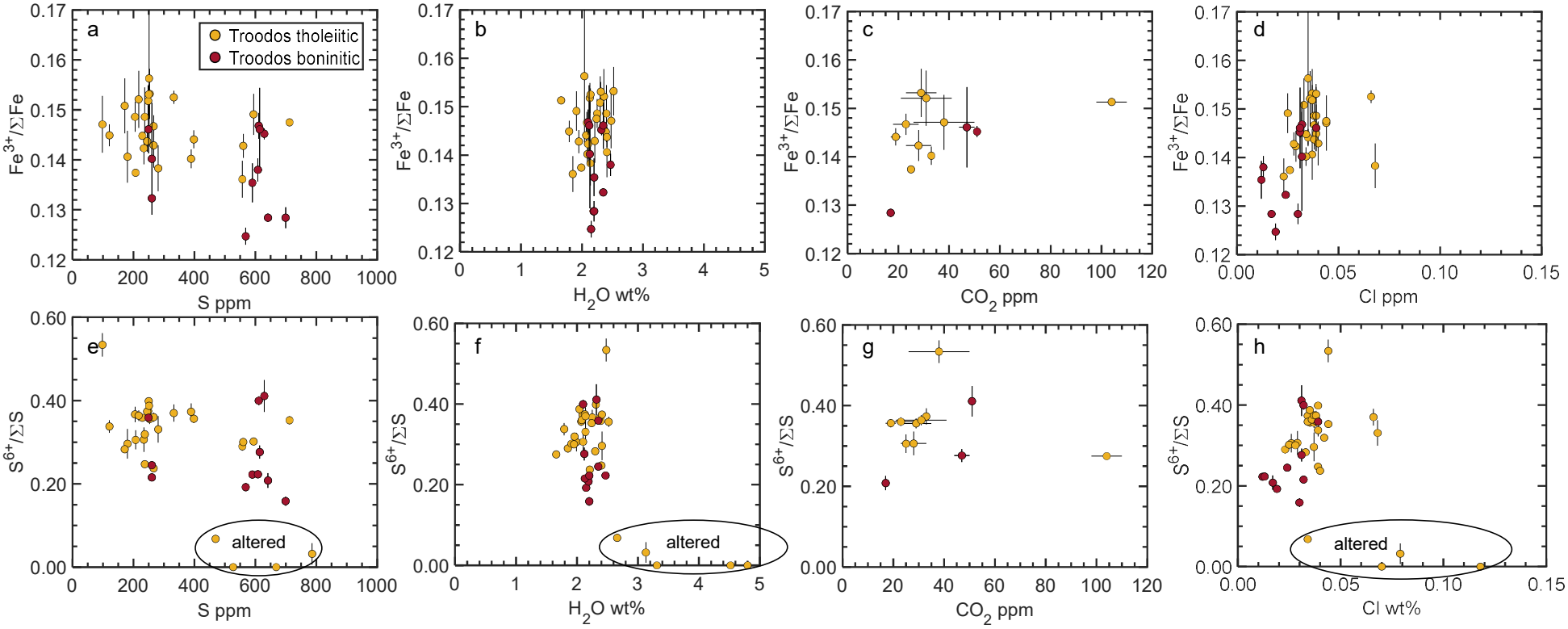

Figure S2. Comparison of volatile elements dissolved in volcanic glasses from the Troodos Ophiolite with XANES measurements of $Fe^{3+}/\Sigma Fe$ (top row) and $S^{6+}/\Sigma S$ (bottom row) in the same glasses. **(a)** and **(e)**: S ppm; **(b)** and **(f)**: H_2O wt.%; **(c)** and **(g)**: CO_2 ppm; **(d)** and **(h)**: Cl wt. %. Volatile element concentrations are from measurements by Woelki et al. (2020) of the same glasses for which XANES measurements were made. In the bottom row, altered glasses measured by S XANES are identified with a labeled ellipse.

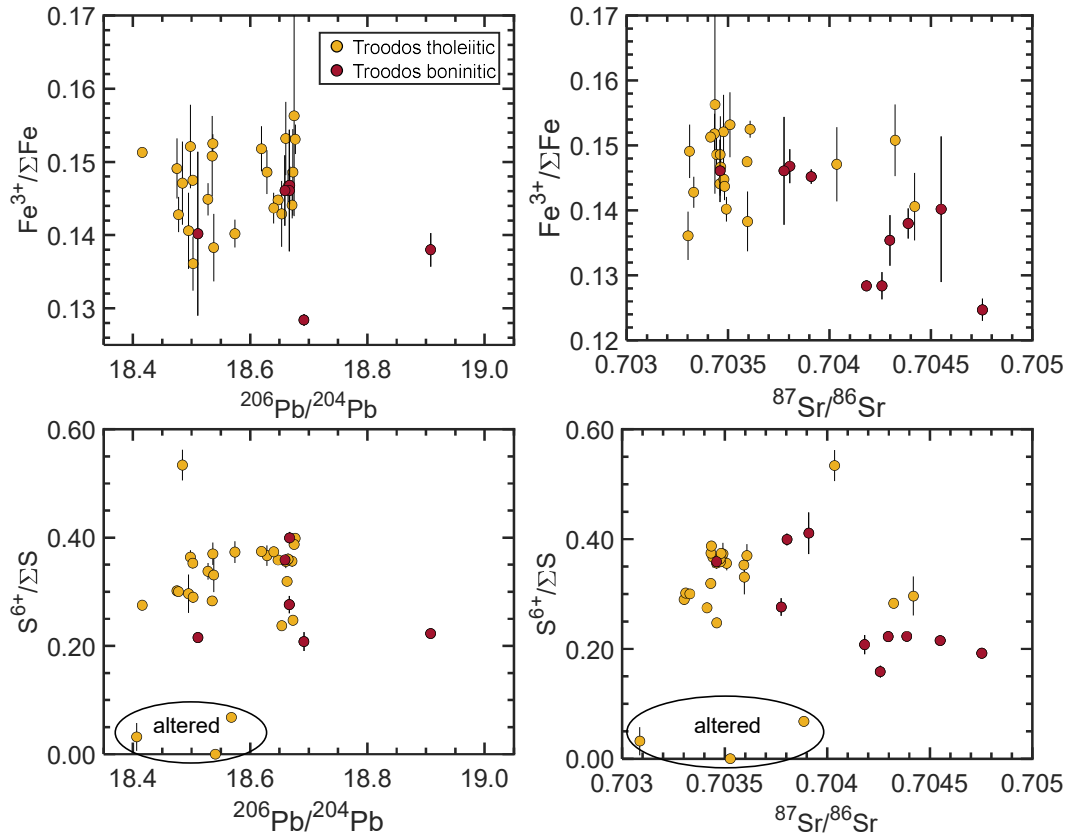

Figure S3. Comparison of volatile elements dissolved in volcanic glasses from the Troodos Ophiolite with XANES measurements of $Fe^{3+}/\Sigma Fe$ (top row) and $S^{6+}/\Sigma S$ (bottom row) in the same glasses. Left column: $^{206}Pb/^{204}Pb$; right column: $^{87}Sr/^{86}Sr$. Isotopic measurements are from Woelki et al. (2020). In the bottom row, altered glasses measured by S XANES are identified with a labeled ellipse.

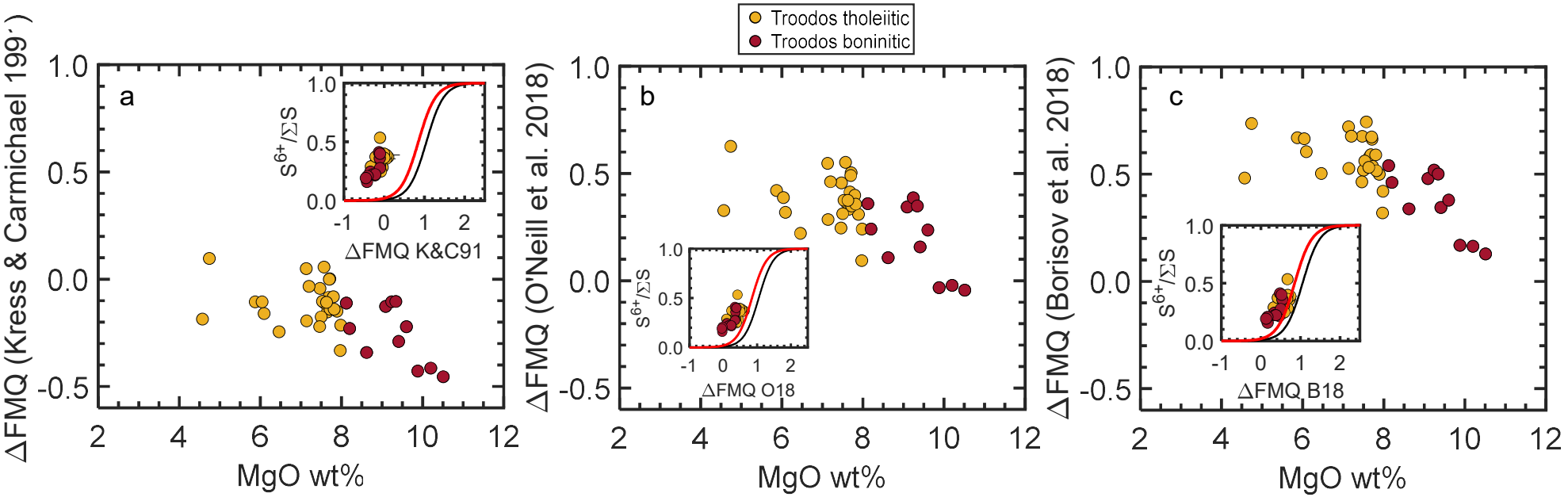

Figure S4. Calculation of fO_2 based on glass Fe^{3+}/Fe^{2+} ratios measured by XANES using three Fe oxybarometers: **(a)** Kress and Carmichael, 1991; **(b)** O'Neill et al., 2018; **(c)** Borisov et al., 2018. fO_2 is expressed relative to the FMβQ buffer of Frost (1991). The insets in each panel compare the calculated fO_2 values to XANES measurements of $S^{6+}/\Sigma S$ in the same glasses. The curves in each inset show two parameterizations of ΔFMQ vs. $S^{6+}/\Sigma S$; the black curve was calculated using the equations in O'Neill and Mavrogenes (2022) evaluated using a composition representative of the boninitic Troodos glasses at T = 1200°C; the red curve is the model of Jugo et al. (2010) for hydrous tholeiite recalculated at 1200°C using the T-dependence of O'Neill and Mavrogenes (2022). Note that for the calculations of O'Neill et al. (2018) shown in panel **(b)**, the Fe XANES data were adjusted to be consistent with the Mössbauer calibration of Berry et al. (2018). The Borisov et al. (2018) model was chosen to calculate fO_2 in the main text because it performed best in simultaneously reconciling Fe and S speciation at a common fO_2 and T (*i.e.,* compare the data to the calculations in each inset).

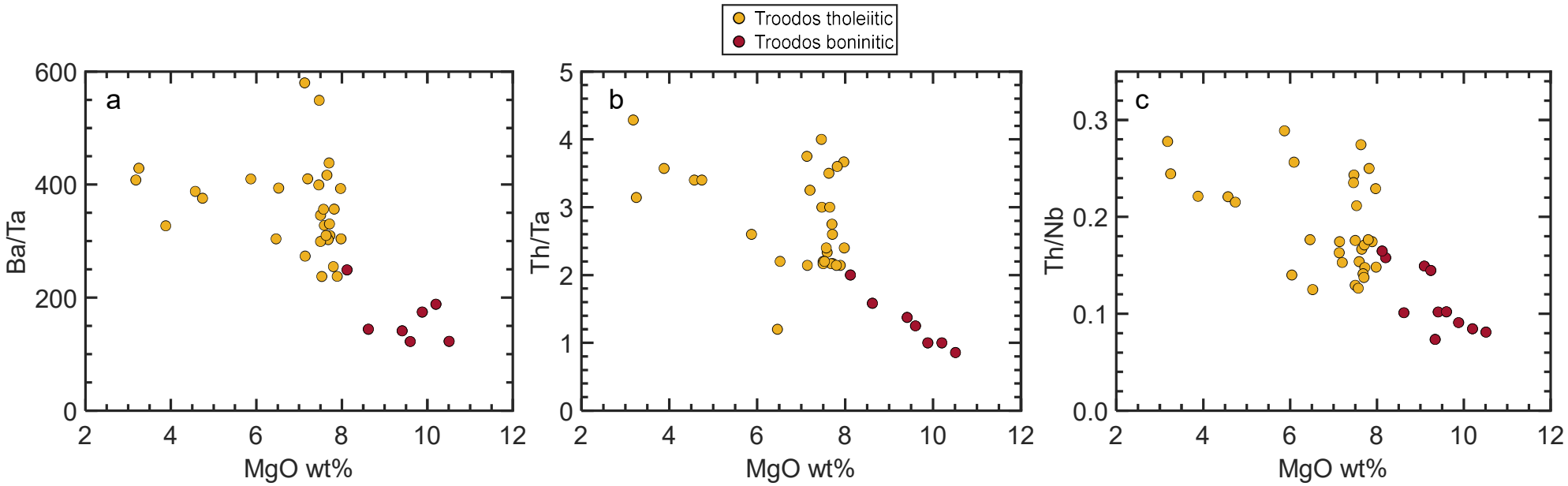

Figure S5. MgO wt.% versus trace element ratios commonly used to track subduction influence (*e.g.,* Pearce et al., 2005) measured in Troodos Ophiolite glasses. **(a)** Ba/Ta; **(b)** Th/Ta; **(c)** Th/Nb. The strong positive correlations of these ratios as a function of MgO contents limit their applicability as proxies for slab influence in our samples with XANES measurements.

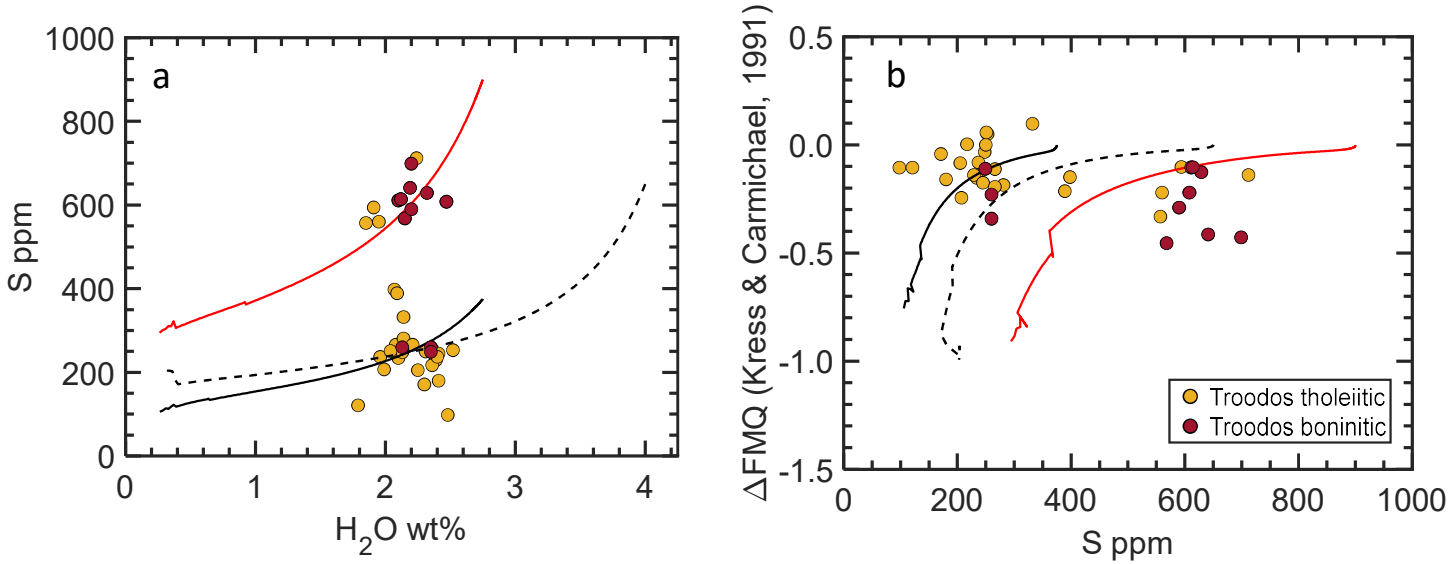

Figure S6. Forward degassing models using the Sulfur_X model (Ding et al., 2023) compared to dissolved volatile contents (Woelki et al., 2020) in the Troodos Ophiolite glasses measured by XANES in this study. **(a)** H_2O wt% vs. S ppm, **(b)** S ppm vs. $ƒO_2$, expressed relative to the FMβQ buffer of Frost (1991), and calculated using Kress and Carmichael, 1991: note that Sulfur_X uses Kress and Carmichael, 1991 to convert between $ƒO_2$ and Fe^{3+}/Fe^{2+}. Each calculation was run at 1200°C in the absence of crystallization, using the Fe-S redox equilibria equations of O'Neill and Mavrogenes (2022). The melt composition was based on measurements of the primitive glass CY16-glass-135 from Kapilio. The initial $ƒO_2$ was set to ΔFMQ=0. The red curve was calculated using initial values of H_2O = 2.75 wt% and S = 900; the black solid curve was calculated using initial H_2O = 2.75 wt% and S = 375 ppm; the black dashed curve uses initial H_2O = 4 wt% and S = 650 ppm. Note that no single degassing model can account for both the high-S and low-S groups of glasses. The models which pass through the data are non-unique, but can plausibly explain the H_2O vs. S systematics of the two groups. Critically, the degassing models produce S vs. $ƒO_2$ paths that are orthogonal to the trends defined by the data, and thus cannot account for the negative correlation between S and $ƒO_2$ shown in panel **(b)**.

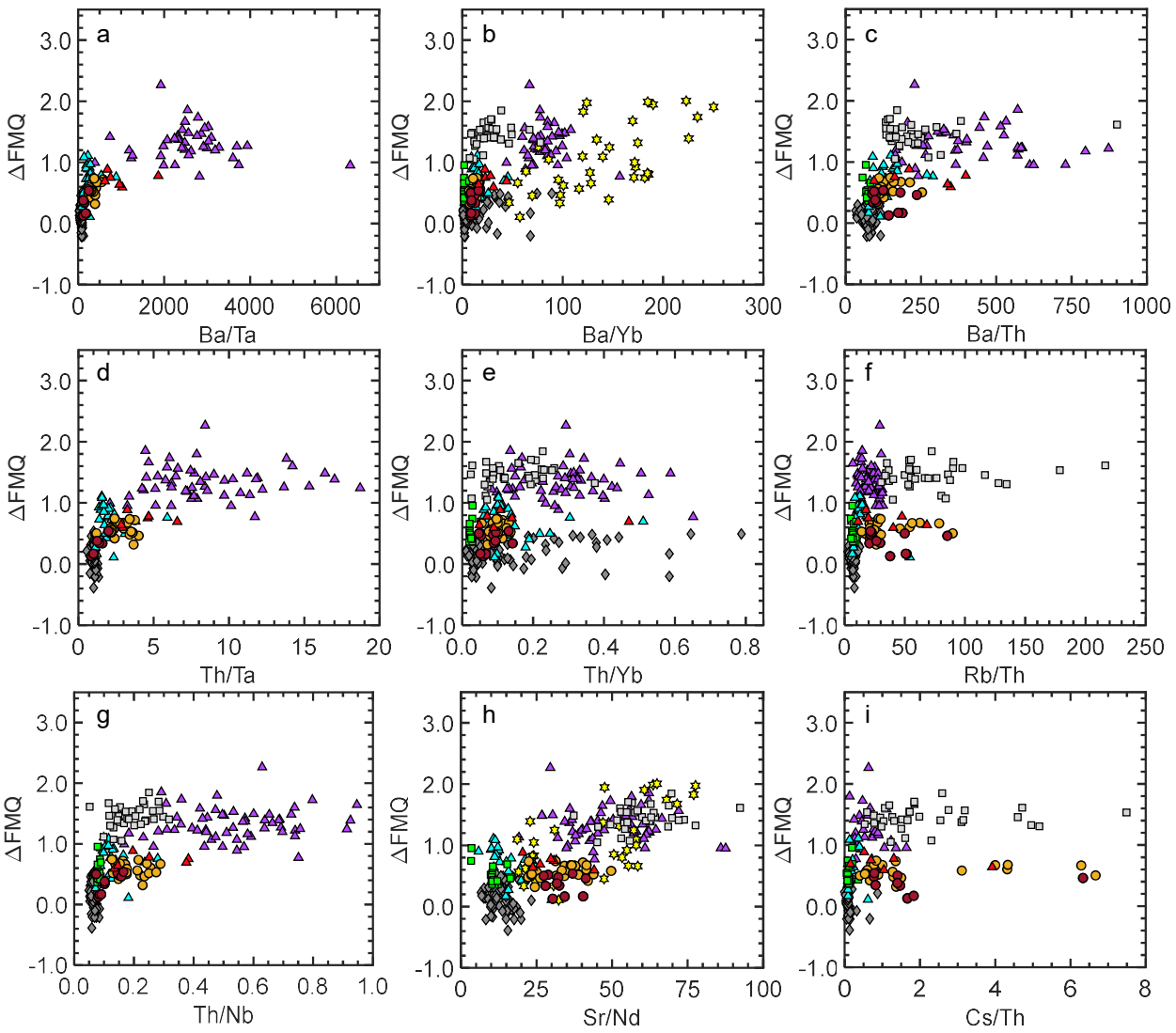

Figure S7. Comparison of trace element proxies for the influence of slab fluids and melts to calculated fO_2 values in our compilation of quenched glasses from the Troodos Ophiolite with Fe XANES measurements. fO_2 is expressed relative to the FMβQ buffer of Frost (1991); calculation details are described in Section 4.1. **(a)** Ba/Ta, **(b)** Ba/Yb, **(c)** Ba/Th, **(d)** Th/Ta, **(e)** Th/Yb, **(f)** Rb/Th, **(g)** Th/Nb, **(h)** Sr/Nd, **(i)** Cs/Th. MI = melt inclusion; all other data are from matrix glasses. MORB: gray diamonds; Izu-Bonin-Mariana (IBM) boninites: gray squares; IBM forearc basalts, green squares; Mariana trough backarc basalts: cyan triangles; Fina Nagu southern Mariana margin: red triangles; purple up-facing triangles; Mariana island-arc melt inclusions: purple triangles; Lassen volcano (Cascade arc) melt inclusions: yellow stars. Data sources: MORB, Kelley and Cottrell, 2009; Cottrell and Kelley, 2011; 2013; Le Voyer et al., 2015, Berry et al., 2018, Birner et al., 2018; Lerner et al., 2021; Mariana arc melt inclusions, Brounce et al., 2014; Fina Nagu, Brouce et al., 2016; IBM boninites and FAB, Brounce et al., 2021; Cascades arc, Lassen segment melt inclusions, Muth and Wallace, 2021; Troodos Ophiolite (this study).

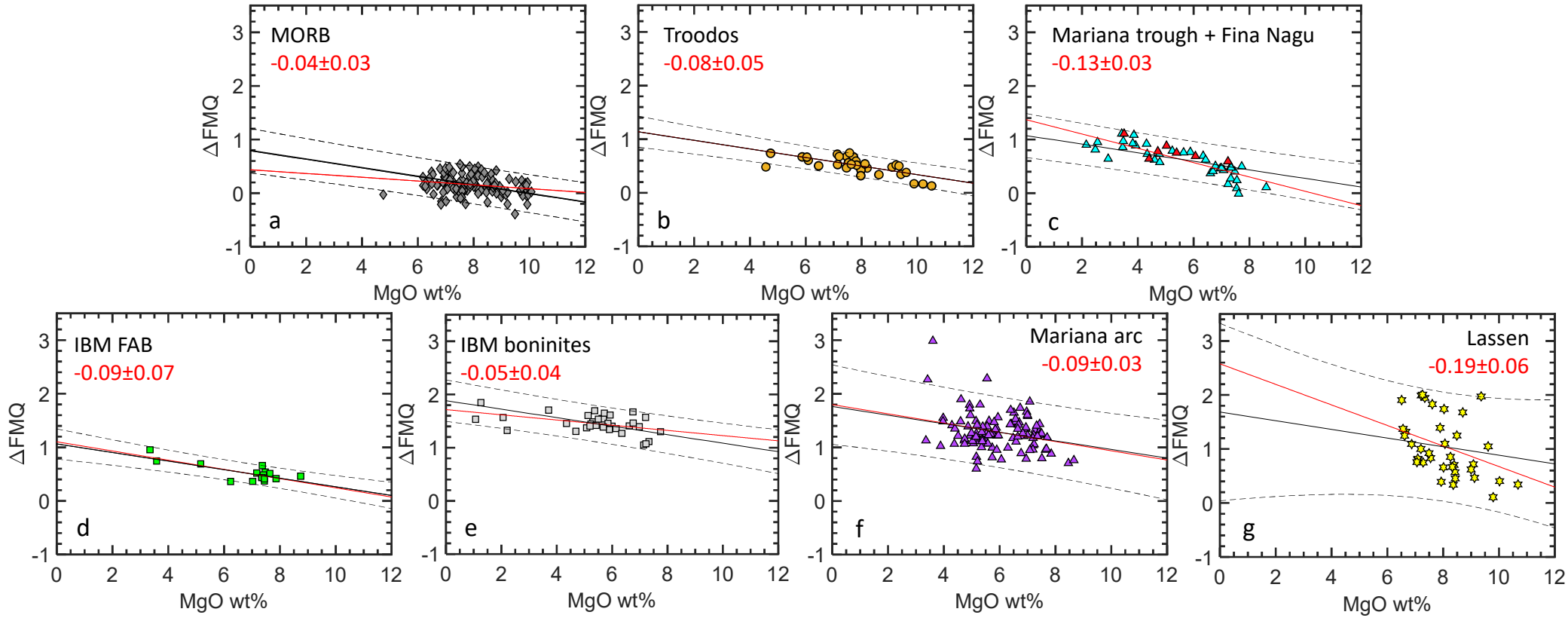

Figure S8. MgO vs. ΔFMQ for each of the tectonic settings in our compilation of glasses with Fe XANES measurements. Black lines were calculated using a fixed slope = –0.08; the dashed lines are 95% prediction intervals, assuming uniform uncertainties. The red curves are best-fit lines to each dataset; the best-fit slope and standard error (1σ) are reported red text. Note that nearly all the data fit within the 95% prediction intervals of the black curve. Comparison of the vertical distance between the black and red curves at MgO = 8 wt.% demonstrates that using a fixed slope of –0.08 versus the best-fit slope makes essentially no difference in the calculated $[\Delta FMQ]_8$ values used in the text. **(a)** MORB; **(b)** Troodos; **(c)** Mariana trough and Fina Nagu; **(d)** Izu-Bonin fore-arc basalts; **(e)** Izu-Bonin boninites; **(f)** Mariana arc melt inclusions, **(g)** Cascades arc melt inclusions, Lassen segment.

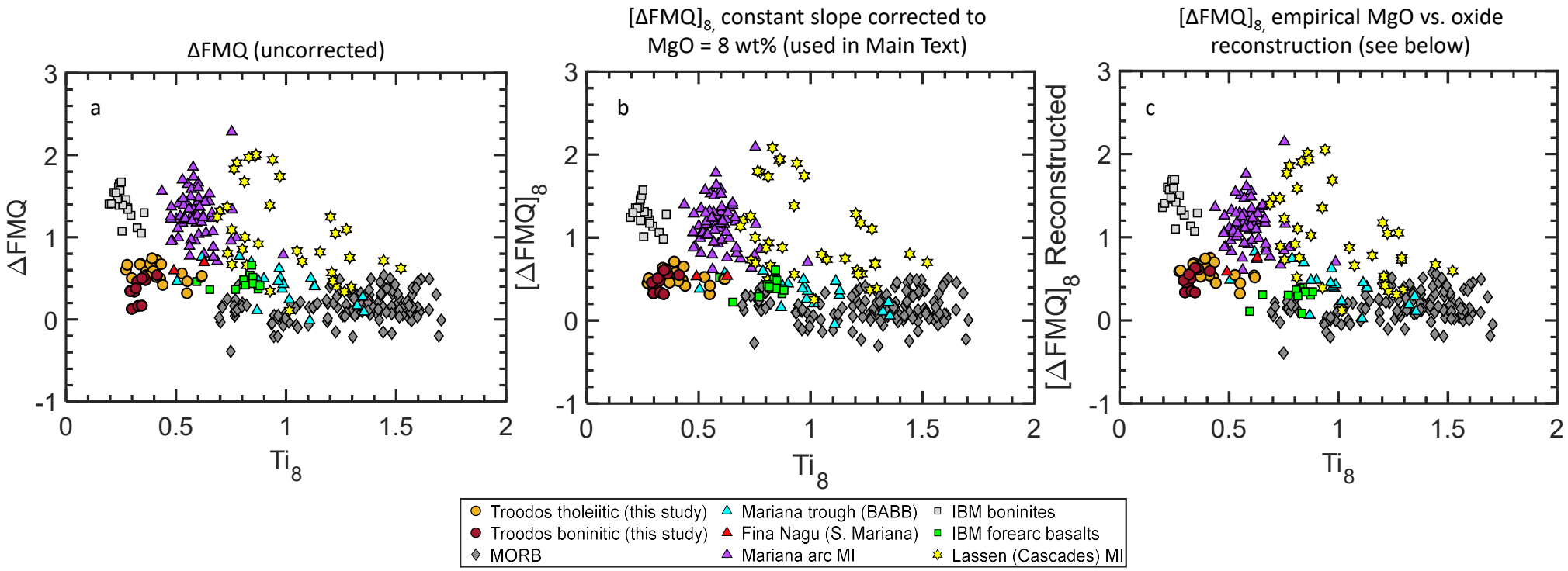

Figure S9. Ti_8 vs. fO_2 expressed as ΔFMQ using three different approaches. **(a)** fO_2 calculated using Borisov et al. (2018) based on glass compositions measured by microprobe, Fe^{3+}/Fe^{2+} ratios measured by XANES, and quench *T* calculated using Putirka (2008) eq. 15. **(b)** fO_2 calculated as in **(a)**, and then adjusted to MgO = 8 wt% using a constant slope of δ[ΔFMQ]/δ[MgO wt%] = –0.08. This is the approach adopted in Section 4.3.3 of the text, *i.e.*, $[\Delta FMQ]_8$. Using the slopes fit individually to each dataset (Fig. S7) results in calculated $[\Delta FMQ]_8$ that are essentially indistinguishable from those shown in panel **(b)**. **(c)** For each location in the compilation, a line was fit to MgO vs. each oxide not represented in the algorithms of Langmuir et al. (2006) and Bézos et al. (2009) and that are represented in the oxybarometer of Borisov et al. (2018) (*i.e.,* SiO_2, Al_2O_3, FeO, Fe_2O_3, CaO, P_2O_5). Each of these oxides was then projected to MgO = 8 wt% using the appropriate fit based on the sample location. The liquidus T was then recalculated using Putirka (2008) eq. 15 and fO_2 was recalculated based on this reconstructed composition using Borisov et al. (2018). This approach likely introduces significant uncertainties due to fitting each oxide separately in each location. Regardless of the approach used, the Ti_8 vs. ΔFMQ systematics presented in the main text are preserved.